Leading-edge–gel coupling in lamellipodium motion

Juliane Zimmermann,[1,*] Mihaela Enculescu,[2] and Martin Falcke[1]

[1]*Mathematical Cell Physiology, Max-Delbrück-Center for Molecular Medicine, Robert-Rössle-Str. 10, 13092 Berlin, Germany*
[2]*Institute for Theoretical Physics, Technische Universität, Hardenbergstraße 36, 10623 Berlin, Germany*

We present a model for actin-based motility that combines the dynamics of the semiflexible region at the leading edge of the lamellipodium with actomyosin gel properties in the bulk described by the theory of active polar gels. We calculate the velocity of the lamellipodium determined by the interaction of the gel and adhesion with forces in the semiflexible region. The stationary concave force-velocity relation of the model reproduces experimental results. We suggest that it is determined by retrograde flow at small forces and gel formation and retrograde flow at large ones. The variety of dynamic regimes of the semiflexible region reproducing experimentally observed morphodynamics is conserved when we couple the leading edge to the gel.

I. INTRODUCTION

The dynamics of the actin cytoskeleton drives the motion of a variety of cell types. In order to crawl, the cell builds a flat lamellipodium at the front [1]. The biopolymer actin forms a dense network inside it. Actin filaments polymerize preferentially at one end and depolymerize at the other, thus generating motion from the hydrolysis of adenosine triphosphate (ATP). Since the actin network is mainly aligned into the direction of motion, the growth of filaments by polymerization leads to a protrusion of the plasma membrane at the leading edge of the cell [2]. The actin network is stabilized by proteins that cross link actin filaments. Typical cross linkers are motor molecules like myosin. They also contract the cytoskeleton and retract the cell body by sliding along the polar filaments.

Two regions of the actin network in the lamellipodium can be distinguished. The bulk consists of long cross-linked filaments [3] and is attached to the substrate by integrins. Since this dense actin network has viscoelastic properties and can be described in a continuum approximation [4], we will call this part actomyosin gel. At the leading edge we find the polymerizing tips of the filaments. The tips are not cross linked yet [3]. We call the range between leading-edge membrane and the average positions of the first cross linkers semiflexible region (SR) (see Fig. 1). The SR width of a few hundred nanometers is small compared to the gel width of typically 10 μm.

The semiflexible region exhibits rich spatiotemporal dynamics. Localized retractions and protrusions of the leading edge traveling along it have been measured indicating an excitable dynamics [5–8]. Spatially modulated oscillatory protrusions and retractions, which are independent from myosin, occur as well [5,8]. A recently developed model for the semiflexible region exhibits all these dynamic regimes [9–11], whereas gel models only show oscillations in the presence of myosin activity or other putative processes generating stress actively. However, microscopic polymer brush models alone cannot determine the cell velocity, since it de-

pends also on the properties of the gel in the bulk of the lamellipodium and adhesion to the substrate. These processes have been successfully modeled in a variety of studies describing the actin network as viscoelastic gel [4,12–17]. But, so far, there is no model reproducing the dynamic regimes of the semiflexible region *and* determining the cell velocity.

The force-velocity relation of motile cells is the relation between lamellipodium velocity and an external force applied to the leading edge. Both semiflexible polymer and gel properties are crucial for its calculation also since longer filaments exert weaker forces. Experiments leading to very broad semiflexible regions and consequently very floppy filaments demonstrate that [18,19]. These experiments also show that gel boundary and leading edge can move independently and therefore both need to be modeled. There have been several models of lamellipodium motion including gel processes and polymerization at the leading edge (but no semiflexible region) [12–17,20]. Prass *et al.* [21] compared them with experiments and concluded that none of them reproduces the force-velocity relation. The measured force-velocity curve has a concave shape: a phase of constant velocity at small forces is followed by a phase of rapidly
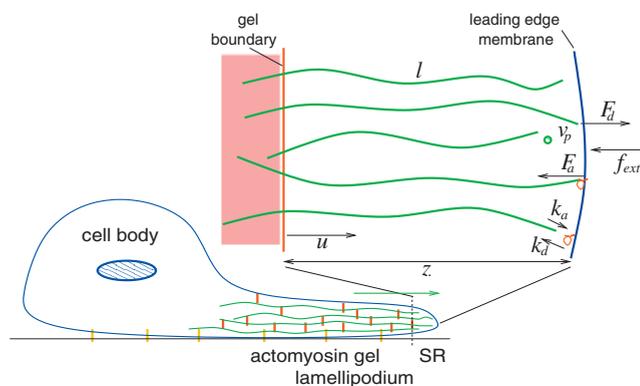

FIG. 1. (Color) In our model, the bulk of the lamellipodium (length ≈ 10 μm) is filled with the actomyosin gel, which is described by a continuum gel model. The polymerizing tips of the actin filaments at the leading edge of the lamellipodium constitute a force and protrusion generating boundary layer (width $\approx$ a few 100 nm). We refer to this part as semiflexible region (SR).

_____
*juliane.zimmermann@mdc-berlin.de

decreasing velocity at larger ones. The ratchet-type model exhibits a convex force-velocity relation, the velocity in the autocatalytic branching model is force independent [22], and the stepping motor model does not take gel properties into account [23]. Recently, a study simulating the force-velocity relation has been published [24] that reproduces the concave-down shape, but stall forces are by a factor of 20–60 too large. This model does not include a semiflexible region and filament attachment to the membrane. We assume that this is the reason for the large stall forces.

In summary, theoretical understanding of both lamellipodium dynamics and the force-velocity relation requires combining semiflexible region and gel dynamics. We use the theory of the active polar gel that was developed by Kruse *et al.* [4] to calculate the flow of the gel. A force boundary condition that is required for this calculation is obtained from the coupling to the semiflexible region. We find that the combined model exhibits the impact of gel properties on the protrusion rate, the rich dynamics of the SR model, and a concave-down force-velocity relation.

II. SEMIFLEXIBLE REGION MODEL

The dynamics of the actin filament tips in the semiflexible region are captured by the following set of equations [9]:

$$\partial_t n_a = k_a n_d - k_d(l_a, z) n_a,$$

$$\partial_t l_d = v_p(l_d, z) - \tilde{v}_g(l_d, z) + k_d(l_a, z)\frac{n_a}{n_d}(l_a - l_d),$$

$$\partial_t l_a = -\tilde{v}_g(l_a, z) + k_a\frac{n_d}{n_a}(l_d - l_a),$$

$$\partial_t z = \frac{1}{\kappa}[n_a F_a(l_a, z) + n_d F_d(l_d, z) - f_{ext}] - u. \quad (1)$$

We consider the number densities of two different filament populations: filaments are either attached to the membrane (n_a) by some protein complex or detached (n_d). The actin gel provides support for the filaments in the semiflexible region, so that they can transfer mechanical momentum to the membrane. The distance between the gel boundary and the membrane is denoted by z. The freely fluctuating part of a filament measured from the gel boundary to the tip is flexed by Brownian motion and can be characterized by its contour length $l_{a/d}$. We assume that all filaments are directed normal to the membrane. If the filament is not attached to the membrane, it pushes the membrane with an entropic force F_d. The probability density distribution $P(z)$ of the filament end-to-end distance defines a free energy $\mathcal{F}(z) = -k_B T \ln P(z)$, from which the average normal force on the membrane can be derived as [25]

$$\langle F_d \rangle(z) = -\frac{\partial \mathcal{F}(z)}{\partial z} = F_c \tilde{F}_d(\tilde{\eta}).$$

The scale of this force is given by the Euler buckling force

$$F_c = k_B T l_p / l_d^2,$$

where l_p denotes the persistence length of the filament [20,26], and the scaling parameter is given by $\tilde{\eta} = l_p(l_d - z)/l_d^2$. In the following, we use the force dependence on contour length and semiflexible region depth $F_d(l_d, z)$ in the weakly bending rod approximation derived in [26]. The derivation shows that for small compression $\tilde{\eta} \lesssim 0.2$ the scaled force reads

$$\tilde{F}_d = \frac{4 \exp\left(-\dfrac{1}{4\tilde{\eta}}\right)}{\pi^{5/2} \tilde{\eta}^{3/2}\left[1 - 2\,\mathrm{erfc}\left(\dfrac{1}{2\sqrt{\tilde{\eta}}}\right)\right]},$$

and for strong compression,

$$\tilde{F}_d = \frac{1 - 3\exp(-2\pi^2\tilde{\eta})}{1 - \dfrac{1}{3}\exp(-2\pi^2\tilde{\eta})}.$$

It is believed that the directionality of cell protrusions is maintained by directed growth [27]. While detached filaments always push the membrane, filaments can, depending on their length, also exert a pulling force during attachment. The molecular details of filament-membrane links are not yet fully understood. We therefore assume that single filaments can transiently attach to the membrane via linker proteins that behave like elastic springs. We distinguish three regimes for the force F_a exerted by the serial arrangement of polymer and linker, depending on the relation between the depth of the semiflexible region z, the equilibrium end-to-end distance $R_{\parallel}$, and the contour length l_a [9]:

$$F_a(l_a, z) = \begin{cases} -k_{\parallel}(z - R_{\parallel}), & z \leq R_{\parallel} & \text{(i)} \\ -k_{eff}(z - R_{\parallel}), & R_{\parallel} < z < l_a & \text{(ii)} \\ -k_l(z - l_a) - k_{eff}(l_a - R_{\parallel}), & z \geq l_a. & \text{(iii)} \end{cases}$$

The three cases correspond to (i) a compressed filament that pushes against the membrane, (ii) filament and linker that pull the membrane while being stretched together, and (iii) a filament that is fully stretched, but the linker continues to pull the membrane by being stretched further. Here, $k_{\parallel}$, k_l, and k_{eff} are the linear elastic coefficients of polymer, linker, and serial polymer-linker arrangement, respectively. For $k_{\parallel}$ we use the linear-response coefficient of a wormlike chain grafted at both ends [28,29], itself a function of polymer stiffness and contour length [29], p. 27.

We assume that nucleation of new filaments and capping of existing ones conserve the total number density n. The density within the semiflexible region is constant in radial direction since we consider only filaments transmitting forces between leading-edge membrane and gel and reaching across the whole semiflexible region. The numbers of attached and detached filaments vary due to transitions between the two populations [see first of Eqs. (1)]. Detached filaments attach to the membrane with a constant attachment rate k_a and attached filaments detach with a force-dependent detachment rate $k_d = k_d^0 \exp(-dF_a/k_B T)$. k_d^0 is the detachment rate if filaments exert no force on the membrane. The length

added by a monomer to the filament is $d=2.7$ nm. The density of detached filaments is $n_d = n - n_a$.

The second and third of Eqs. (1) comprise the variation of the filaments' average contour lengths. The length of detached filaments l_d increases by polymerization. The polymerization velocity is force dependent [20]: $v_p = v_p^{max} \exp(-dF_d/k_B T)$. The force-free polymerization velocity v_p^{max} is determined by the concentration of actin monomers in the semiflexible region. It can be assumed that the pool of monomers is maintained by the buffering function of profilin and diffusion from the bulk.

The length of filaments decreases by growth of the actin gel. The gel boundary advances by microscopic processes causing gelation like cross linking of newly polymerized filaments and entanglement. We call the actin network a gel, when a critical concentration of cross linkers has been reached. The cross-linking velocity v_g depends on the contour length. It vanishes for $l \rightarrow 0$ since cross linkers cannot bind when $l=0$. It increases with increasing l and saturates due to limited cross-linker supply. As shown in the Appendix, it can be written as $v_g(l) = v_g^{max} \tanh(l/\bar{l})$. The characteristic length $\bar{l}$ is inversely proportional to the filament density, and the saturation velocity v_g^{max} is proportional to filament density and cross-linker concentration. If filaments are buckled ($l>z$), progression of the gel consumes l/z times more contour length of filaments than the distance traveled in the laboratory frame. That causes the factor $\max(1, l/z)$ in the rate of filament shortening $\tilde{v}_g(l,z) = \max(1, l/z) v_g(l)$ [9,10]. The last term of the l_d dynamics describes the change of the average length of detached filaments due to detachment of attached filaments. The dynamics of l_a is analogous but lacks polymerization.

The fourth equation describes the dynamics of the distance z. The velocity of the membrane is proportional to the total force exerted on it, i.e., the sum of an external force density f_{ext} and the force from all filaments. All friction forces or viscous drag counteracting membrane motion is captured by the drag coefficient κ. The force exerted by the filaments in the semiflexible region on the membrane acts also on the gel front. That will provide us with the force boundary condition required to calculate the gel flow. We calculate the velocity u of the gel front in the laboratory frame with the theory developed by Kruse *et al.* [4] that captures viscoelastic properties of the actin network, polarization of the network due to alignment of filaments into the direction of motion, and active contractions of the network by myosin [see Eqs. (2)–(4)].

III. GEL MODEL

We use the simplified one-dimensional equations derived in [4,30]. Taking a radial cross section through the lamellipodium and averaging over its height (thin-film approximation) yields the constitutive equation [30]

$$\frac{dv}{dx} = \frac{1}{4\eta}\left(\frac{f(x)}{h(x)} - \mu\right), \tag{2}$$

with the gel viscosity η and the active contractile stress μ from motor molecules. Stress in the gel is described by the

force $f(x)$. $h(x)$ is the height of the gel film and $v(x)$ is the flow field in the laboratory frame. We neglect inertial forces in the force balance

$$\frac{df}{dx} = \xi v(x), \tag{3}$$

where ξ is the friction coefficient of the gel with the substrate, which also describes adhesion [30].

Equations (2) and (3) can be solved when boundary conditions for the force at the gel front $f(0)=f_0$ and at the cell body $f(L)=f_L$ are specified and an expression for the height profile $h(x)$ is given. This expression can be obtained from integrating the continuity equation

$$\frac{d}{dx}\{[v(x) + v_{link} - v(0)]h(x)\} = h_0 v_{link}\delta(x). \tag{4}$$

The gel is produced at the gel front $x=0$ [with height $h(0) = h_0$] by cross linking the filaments of the semiflexible region with a velocity v_{link}. The velocity of the gel front is given by $u = v_{link} - v(0)$. We use the same velocity definition as that of Kruse *et al.*, i.e., $v(x)$ is directed opposite to u and v_{link}.

In conjunction with the semiflexible region model, we will use Eqs. (2)–(4) for the gel behavior in a quasisteady approximation. Some cells like, e.g., keratocytes move with a stationary shape of the lamellipodium, but in others the semiflexible region dynamics may become nonstationary. Our results indicate that even when the plasma membrane shows an oscillatory movement, the gel still moves with a constant velocity in a wide parameter range (see below). Additionally we performed calculations using a time-dependent continuity equation and could show that a stationary solution for the height profile $h(x,t)$ is usually reached after a few seconds, a short time scale compared to oscillation periods. We conclude that the assumption of a quasistationary gel profile is a good approximation, even when we couple the gel to the semiflexible region dynamics.

Solving the gel model: Retrograde flow

To obtain an expression for the gel boundary velocity u that depends on force boundary conditions and gel parameters, we scale Eqs. (2)–(4) by using

$$v' = \frac{v}{v_{link}}, \quad x' = \frac{x}{L}, \quad f' = \frac{f}{L\xi v_{link}}.$$

Using Eq. (4), the differential equation (2) can be written as

$$\frac{dv}{dx} = \frac{1}{4\eta}\left(\frac{f(x)(v(x) + u)}{h_0 v_{link}} - \mu\right).$$

With Eq. (3), we get

$$\frac{d^2 f'}{dx'^2} = \nu_1 f'\left(\frac{df'}{dx'} + 1 - \frac{df'}{dx'}\bigg|_0\right) - \nu_2$$
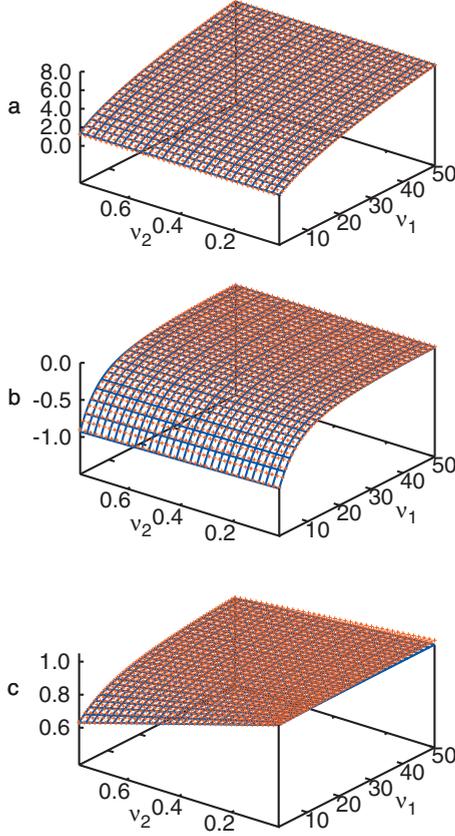
and the scaling parameters

FIG. 2. (Color) Parameters a, b, and c of the fit $u' = af'(0) + bf'(1) + c$ as functions of ν_1 and ν_2. Blue crosses: numerical solutions; red lines: fitting functions (5). Fits and numerical solutions are so close that they are almost undistinguishable in the plots.

$$\nu_1 = \frac{\xi L^2}{h_0 4 \eta}, \quad \nu_2 = \frac{\mu L}{4 \eta v_{link}}.$$

We now solve this equation numerically for different ν_1's and ν_2's as well as different force boundary conditions $f'(0)$ and $f'(1)$. Solving the boundary value problem demands finding the root of a function of $\frac{df'}{dx'}\big|_0$. The velocity u' is then given by $1 - \frac{df'}{dx'}\big|_0$.

It can be seen that, in good approximation, u' depends linearly on $f'(0)$ and $f'(1)$. We therefore assume that u' has the form $u' \approx af'(0) + bf'(1) + c$ and determine the coefficients a, b, and c for different parameters ν_1 and ν_2. The results are shown in Fig. 2. a, b, and c have been fit as functions of ν_1 and ν_2 by

$$a = (1 + 0.92\nu_1)^{1/2}(1 + 0.03\nu_2),$$

$$b = -\frac{1 + 0.1\nu_2}{1 + 0.15\nu_1 + 0.013\nu_1^2},$$

$$c = 1 - \frac{\nu_2}{2 + 0.12\nu_1}. \tag{5}$$

Scaling back to physical units yields

$$u \approx v_{link} - \frac{\mu L}{4\eta}g_1 + \frac{f_0}{L\xi}g_2 - \frac{f_L}{L\xi}g_3,$$

$$g_1 = \frac{1}{2.0 + 0.12\dfrac{\xi L^2}{4\eta h_0}},$$

$$g_2 = \left(1.0 + 0.92\frac{\xi L^2}{h_0 4\eta}\right)^{1/2}\left(1.0 + 0.03\frac{\mu L}{4\eta v_{link}}\right),$$

$$g_3 = \frac{1.0 + 0.1\dfrac{\mu L}{4\eta v_{link}}}{1.0 + 0.15\dfrac{\xi L^2}{h_0 4\eta} + 0.013\left(\dfrac{\xi L^2}{h_0 4\eta}\right)^2}. \tag{6}$$

We have fit g_1, g_2, and g_3 for $0 \le \xi L^2/4\eta h_0 \le 50$. Equations (6) are valid on the condition that $\mu L/4\eta v_{link} < 1$ since the solution of the gel equations (2)–(4) diverges at finite L [31].

The gel front moves slower than the cross-linking velocity v_{link} since the gel flows backward. This is called retrograde flow and is observed in moving cells [7,32–34]. The second term on the right-hand-side of Eqs. (6) characterizes the retrograde flow due to contraction by myosin motors in the absence of external forces. Contraction slows down or (depending on other parameters) even retracts the gel front in agreement with experimental observations. The term proportional to f_0 reflects the retrograde flow due to filaments of the semiflexible region pushing against the gel front. A negative value of f_0 corresponds to a pushing force, which increases the retrograde flow and decreases the gel velocity u. The retrograde flow is fast for small $L\xi$ since the gel does not have the grip to stand the force exerted by the boundary layer. The cell will slow down or stop. Increasing $L\xi$ increases the cell velocity by providing grip with the substrate. Similarly, increasing the viscosity also increases u since the gel provides better support for pushing the membrane.

The factor g_3 of the force at the cell body f_L decreases quickly with increasing friction ξ and length of the lamellipodium. That illustrates the absorption of forces at the back by adhesion sites. At realistic parameter values (see Table I) $g_2/g_3 \approx 40$ holds, i.e., the effect of f_0 on the gel boundary velocity is much larger than the one of f_L. Therefore, we will use $f_L = 0$ in the following.

IV. RESULTS OF THE COUPLED MODEL

The lamellipodium velocity is obtained by numerically solving the semiflexible region model (1) with Eqs. (6) as the velocity of the gel front. The force boundary condition is $f_0 = -[n_a F_a(l_a, z) + n_d F_d(l_d, z)]$ and v_{link} equals the average cross-linking velocity $[n_a v_g(l_a) + n_d v_g(l_d)]/n$. We find stationary, bistable, excitable, and oscillatory regimes of leading-edge motion. An oscillatory solution is plotted in Fig. 3. In stationary regimes, $\partial_t z = 0$ and $f_0 = -\kappa u - f_{ext}$ hold. Therefore, we obtain

TABLE I. List of model parameters and their values in Figs. 3 and 4.

Symbol	Meaning	Value	Unit	Reference
n	Total filament density	300	μm^{-1}	[35]
k_a	Attachment rate of filaments to membrane	0.3	s^{-1}	10/s in [36]
k_d^0	Detachment constant	0.167	s^{-1}	0.5/s in [37]
v_p^{max}	Saturation value of polymerization velocity	15 (Fig. 3), 6 (Fig. 4)	$\mu m/min$	[20,35,38]
v_g^{max}	Saturation value of gel cross-linking velocity	3	$\mu m/min$	Assumed
$\bar{l}$	Saturation length of cross-linking velocity	0.1	μm	Assumed
κ	Drag coefficient of plasma membrane	0.833	$nN\, s/\mu m^2$	[39]
d	Actin monomer radius	2.7	nm	[40]
l_p	Persistence length of actin	15	μm	[41]
k_l	Spring constant of linker protein	1	$nN/\mu m$	[37,42]
η	Viscosity of actin gel	50	$nNs/\mu m^2$	270 $nN\, s/\mu m^2$ in [30], 10 $nN\, s/\mu m^2$ in [14]
ξ	Friction coefficient of actin gel to substrate	1.66–8.33	$nNs/\mu m^3$	30 $nN\, s/\mu m^3$ in [30], 1 $nN\, s/\mu m^3$ in [14]
μ	Active contractile stress in actin gel	27.8	$pN/\mu m^2$	Assumed
h_0	Height of lamellipodium at leading edge	0.1	μm	[35,43,44]
L	Length of gel part of lamellipodium	10	μm	[3,44]
f_0	Force at cell body	0		Assumed

$$u = \frac{v_{link}(f_{ext},\kappa) - \frac{\mu L}{4\eta}g_1 - \frac{f_{ext}}{\xi L}g_2 + \frac{f_L}{\xi L}g_3}{1 + \frac{\kappa}{\xi L}g_2}. \qquad (7)$$

The dependence of the average membrane velocity on external force f_{ext} is shown in Fig. 4. The curves show a distinct change in slope. In the range with small slope, v_{link} depends only weakly on the external force since the free length of polymer in the semiflexible region is larger than the characteristic length $\bar{l}$ of its l dependence. The membrane velocity depends only via the term $f_{ext}g_2/\xi L$ on the external force, and f_{ext} only speeds up retrograde flow [Fig. 4(c)]. For strong adhesion (large ξ), the external force term in Eq. (7) decreases and the membrane velocity becomes almost constant. When the force increases, filaments in the semiflexible region become shorter in order to be able to transmit the force to the gel and in accordance with the length dependence of F_a and F_d. The polymer length approaches $\bar{l}$, v_{link} decreases, and the slope of the force-velocity relation becomes steep. The external force also hampers gel formation now.
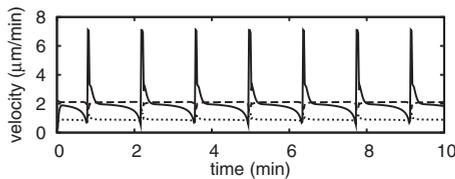
FIG. 3. Example for an oscillatory solution of system (1) using Eq. (6) for u: membrane velocity (solid line), velocity of gel front (dashed line), and retrograde flow (dotted line). f_{ext} =0.125 nN s/μm, k_a=18 min^{-1}, k_d^0=10 min^{-1}, v_g^{max}=3 μm/min, v_p^{max}=15 μm/min, κ=0.05 kg/(μm min), n=300 μm^{-1}, μ =27.8 pN/μm^2, ξ=0.2 kg/(μm^2 min), η=5 kg/(μm min), L =10 μm, h_0=0.1 μm, and f_L=0. See also Table I.

The membrane velocity oscillates at small external forces, because the stationary state becomes unstable with respect to perturbations of n_a. Decreasing the number of attached filaments increases the load on the remaining ones accelerating their detachment also. The pulling force n_aF_a drops to very small values and the membrane jerks forward. This instability with respect to n_a perturbations is crucial for the oscillation mechanism (see [9,10] for details).

The viscous force κu can slow down the lamellipodium also, but in difference to f_{ext} does not cause negative u [Fig. 4(b)]. We obtain also a transition from stationary to oscillatory movement and the slope change due to the saturation of
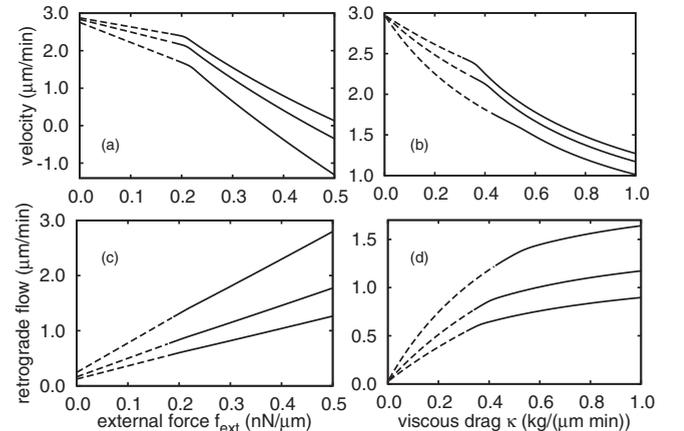
FIG. 4. [(a) and (b)] Mean membrane velocity and [(c) and (d)] retrograde flow as functions of [(a) and (c)] external force f_{ext} applied to the [(a) and (c)] membrane and [(b) and (d)] drag coefficient for three different friction coefficients ξ of the gel to the substrate. The membrane velocity increases with ξ, while retrograde flow decreases: ξ_1=0.2 kg/(μm^2 min), ξ_2=0.5 kg/(μm^2 min), ξ_3 =1.0 kg/(μm^2 min), v_p^{max}=6 μm/min, and f_{ext}=0 in (b) and (d); other parameters are same as in Fig. 3. See also Table I. Solid curve: stationary movement; dashed curve: oscillatory movement.

the gel formation velocity. For $\kappa \to 0$ and $f_{ext}=f_L=0$, the viscous force vanishes and retrograde flow is driven by contraction alone $u=v_{link}-\frac{\mu L}{4\eta}g_1$. If there is no contraction ($\mu=0$) but a viscous force, it drives retrograde flow.

V. SUMMARY AND CONCLUSIONS

We arrive at the picture that the semiflexible region sets the dynamic regime, and gel properties and the forces acting on the leading edge determine the retrograde flow and lamellipodium velocity. Since in oscillatory regimes the viscous and external forces on the membrane are small, retrograde flow is primarily generated by myosin motors and stays constant although the plasma membrane moves with oscillating velocity. Such a behavior has been observed experimentally in growth cone advancement [45].

In agreement with our results, it has been shown experimentally that retrograde flow increases (cell velocity decreases) with myosin motor activity [7,33]. The cell velocity increases with adhesiveness in our model and in experiments [34,46]. It decreases in experiments at very strong adhesion again, which is not reproduced by the model, since we did not include the coupling from cell back to front required for that.

Our model offers a simple and biologically plausible explanation for the concave-down shape of the force-velocity relation. Our force-velocity relation for strong adhesion shows a shape similar to experimental results [21,47] and gives quantitatively correct stall forces. We assume that the autocatalytic branching model [22] would provide a force-velocity relation very similar to ours if it would be combined with a gel model.

As mentioned above, experimentally observed force-velocity relations are almost constant for small forces and decrease faster for larger forces. We obtain this dependency when adhesion is strong (ξ large) and the cross-linking rate is at its saturation value without external force, i.e., $v_p^{max} > v_g^{max}$. The first condition is obviously met since otherwise the cell would slide backward on the substrate at small external forces. It is generally believed that protrusion is force limited [48]. Therefore, the force-free polymerization rate is even faster than observed cell velocities, which shows that the second condition applies also.

When including retrograde flow into the semiflexible region model, different dynamic regimes, stationary movement, and oscillations of the plasma membrane are conserved. We have shown previously that our semiflexible region model describes velocity oscillations of the lamellipodium leading edge and localized protrusions traveling along the edge [5,11]. For small values of the membrane resistance κ, the dynamic regime of movement does not change when we vary the parameters of the gel that determine the strength of the retrograde flow. In good agreement with this result, experiments showed that the state of movement of newt lung epithelial cells did not change when myosin activity, one of the driving factors of retrograde flow, was inhibited [5]. On the whole at parameter values suggested by others to apply to experiments [14,30] (see also Table I), the dynamic regime is determined by processes in the semiflexible region, and

retrograde flow, adhesion, and actin gel properties determine the velocity of the lamellipodium. Our modeling approach allows for describing the impact of the gel in the bulk on membrane motion by a single algebraic expression [Eq. (6)], whenever the gel model by Kruse *et al.* applies. This is a tremendous simplification compared to simulating the complete gel equations throughout the bulk.

APPENDIX: DERIVATION OF CROSS-LINKING RATE

The transition from the semiflexible region with little cross links to the gel with many cross links occurs gradually. The concentration of cross linkers bound to the actin network C_b is saturated far inside the gel and decreases toward the leading-edge membrane to zero since newly polymerized filament parts have no cross-linker bound yet. We denote as the gel boundary the position of a concentration value C_b^{crit}, above which we expect gel-like behavior of the network. We calculate the cross-linking velocity v in stationary state with steady motion. We consider a reference frame along the contour length of a filament in which the gel boundary is fixed. The tip of the filament is located at $x=0$ and the gel boundary is at $x=-l$. We denote with L_G the width of the gel region of the lamellipodium close to the gel boundary where C_b is not saturated yet. C_f is the concentration of free cross linkers. We have a pool of cross linkers in the cell body of constant concentration C_f^{cb}. We use a constant binding rate of cross linkers in order to obtain linear analytically solvable differential equations for the concentrations. We describe binding of cross linkers in the SR by the rate p and binding inside the gel by p_G with $p_G \le p$. That allows taking partial saturation of binding sites inside the gel into account. The stationary spatial distributions of bound and unbound cross linkers are described by

$$D\frac{\partial^2 C_f}{\partial x^2} - p_G C_f = 0, \quad \text{gel},$$

$$D\frac{\partial^2 C_f}{\partial x^2} - p C_f = 0, \quad \text{SR},$$

$$v\frac{\partial C_b}{\partial x} + p C_f = 0, \quad \text{SR}, \tag{A1}$$

with the diffusion coefficient D. Boundary conditions at the gel boundary guarantee a continuous and smooth function C_f. Additionally, we require

$$C_f[-(L_G+l)]=C_f^{cb}, \quad \left.\frac{\partial C_f}{\partial x}\right|_{x=0}=0. \tag{A2}$$

The solution for C_f in the SR $-l \le x \le 0$ is given by

$$C_f = \frac{GC_f^0 \cosh(kx)}{k\sinh(kl) + G\cosh(kl)}, \quad k=\sqrt{\frac{p}{D}},$$

$$G = \frac{k_G}{\tanh(k_G L_G)}, \quad C_f^0 = \frac{C_f^{cb}}{\cosh(k_G L_G)}, \quad k_G = \sqrt{\frac{p_G}{D}}.$$
(A3)

With the boundary condition $C_b(0) = 0$, the solution for the bound cross-linker concentration inside the SR reads

$$C_b = -\frac{p}{vk} \frac{G C_f^0 \sinh(kx)}{k \sinh(kl) + G \cosh(kl)}.$$
(A4)

Reaching the critical concentration of cross linkers bound to filaments C_b^{crit}, above which the actin network becomes a gel, defines the gel boundary $x = -l$ and we can write

$$\frac{p}{vk} \frac{G C_f^0 \sinh(kl)}{k \sinh(kl) + G \cosh(kl)} = C_b^{crit}.$$
(A5)

The cross-linking velocity is then given by

$$v = \frac{p}{C_b^{crit} k} \frac{G C_f^0 \tanh(kl)}{k \tanh(kl) + G}.$$
(A6)

We assume that the binding rate p is proportional to the filament density n squared since filaments have to get sufficiently close to each other to cross link: $p = bn^2$. That yields in the limit $G \gg k \tanh(kl)$

$$v = \frac{n C_f^0 \sqrt{Db}}{C_b^{crit}} \tanh(nl\sqrt{b/D}).$$
(A7)

The contour length in the semiflexible region rarely approaches zero. Even when the leading-edge motion is stalled, retrograde flow maintains a SR and the cross-linking velocity compensates for the flow. Nevertheless, we would like to add a remark applying to the case $l \to 0$. We need to take into account that cross-linker binding sites are located at average distances l_b along the filament if l becomes smaller than l_b. For $l \ll l_b$, the probability to find a cross linker between $x = 0$ and $x = -l$ is l/l_b. That probability turns the cross-linker binding rate into $p = bn^2 l/l_b$. Therefore, the cross-linking velocity (A6) then reads

$$v = \frac{\sqrt{Dbl/l_b}\, n C_f^0 G}{C_b^{crit}} \frac{\tanh[n\sqrt{bl^3/(Dl_b)}]}{\sqrt{bl/(Dl_b)}\, \tanh[n\sqrt{bl^3/(Dl_b)}] + G}.$$
(A8)

[1] D. Bray, *Cell Movements—From Molecules to Motility*, 2nd ed. (Garland, New York, 2001).

[2] R. Ananthakrishnan and A. Ehrlicher, Int. J. Biol. Sci. **3**, 303 (2007).

[3] T. M. Svitkina, A. B. Verkhovsky, K. M. McQuade, and G. G. Borisy, J. Cell Biol. **139**, 397 (1997).

[4] K. Kruse, J. F. Joanny, F. Jülicher, J. Prost, and K. Sekimoto, Eur. Phys. J. E **16**, 5 (2005).

[5] M. Machacek and G. Danuser, Biophys. J. **90**, 1439 (2006).

[6] A. Ponti, M. Machacek, S. L. Gupton, C. M. Waterman-Storer, and G. Danuser, Science **305**, 1782 (2004).

[7] P. Vallotton, G. Danuser, S. Bohnet, J.-J. Meister, and A. B. Verkhovsky, Mol. Biol. Cell **16**, 1223 (2005).

[8] H.-G. Dobereiner, B. J. Dubin-Thaler, J. M. Hofman, H. S. Xenias, T. N. Sims, G. Giannone, M. L. Dustin, C. H. Wiggins, and M. P. Sheetz, Phys. Rev. Lett. **97**, 038102 (2006).

[9] A. Gholami, M. Falcke, and E. Frey, New J. Phys. **10**, 033022 (2008).

[10] M. Enculescu, A. Gholami, and M. Falcke, Phys. Rev. E **78**, 031915 (2008).

[11] M. Enculescu, M. Sabouri-Ghomi, G. Danuser, and M. Falcke, Biophys. J. **98**, 1571 (2010).

[12] M. A. Gracheva and H. G. Othmer, Bull. Math. Biol. **66**, 167 (2004).

[13] F. Gerbal, P. Chaikin, Y. Rabin, and J. Prost, Biophys. J. **79**, 2259 (2000).

[14] K. Larripa and A. Mogilner, Physica A **372**, 113 (2006).

[15] A. T. Dawes and L. Edelstein-Keshet, Biophys. J. **92**, 744 (2007).

[16] S. I. Nishimura, M. Ueda, and M. Sasai, PLOS Comput. Biol. **5**, e1000310 (2009).

[17] E. Kuusela and W. Alt, J. Math. Biol. **58**, 135 (2009).

[18] J. E. Bear *et al.*, Cell **109**, 509 (2002).

[19] S. A. Koestler, S. Auinger, M. Vinzenz, K. Rottner, and J. V. Small, Nat. Cell Biol. **10**, 306 (2008).

[20] A. Mogilner and G. Oster, Biophys. J. **71**, 3030 (1996).

[21] M. Prass, K. Jacobson, A. Mogilner, and M. Radmacher, J. Cell Biol. **174**, 767 (2006).

[22] A. E. Carlsson, Biophys. J. **84**, 2907 (2003).

[23] R. B. Dickinson, L. Caro, and D. L. Purich, Biophys. J. **87**, 2838 (2004).

[24] C. H. Schreiber, M. Stewart, and T. Duke, Proc. Natl. Acad. Sci. U.S.A. **107**, 9141 (2010).

[25] E. Frey, K. Kroy, J. Wilhelm, and E. Sackmann, *Dynamical Networks in Physics and Biology* (Springer Verlag, Berlin, 1998).

[26] A. Gholami, J. Wilhelm, and E. Frey, Phys. Rev. E **74**, 041803 (2006).

[27] M.-F. Carlier and D. Pantaloni, J. Biol. Chem. **282**, 23005 (2007).

[28] K. Kroy and E. Frey, Phys. Rev. Lett. **77**, 306 (1996).

[29] K. Kroy, *Viskoelastizität von Lösungen halbsteifer Polymere* (Hieronymus, Müchen, 1998).

[30] K. Kruse, J. F. Joanny, F. Jülicher, and J. Prost, Phys. Biol. **3**, 130 (2006).

[31] Despite that condition, there is a solution at $v_{link} = 0$, with $v(x) = -u$, $u = (f_0 - f_L)/(L\xi)$, and $h(x) = \mu f(x)$, i.e., contraction forces exactly balance $f(x)$, and motion arises for $f_0 - f_L \neq 0$ only.

[32] C. H. Lin and P. Forscher, Neuron **14**, 763 (1995).

[33] C. H. Lin, E. M. Espreafico, M. S. Mooseker, and P. Forscher, Neuron **16**, 769 (1996).

[34] C. Jurado, J. R. Haserick, and J. Lee, Mol. Biol. Cell **16**, 507 (2005).

[35] V. C. Abraham, V. Krishnamurthi, D. L. Taylor, and F. Lanni, Biophys. J. **77**, 1721 (1999).

[36] J. W. Shaevitz and D. A. Fletcher, Proc. Natl. Acad. Sci. U.S.A. **104**, 15688 (2007).

[37] A. Mogilner and G. Oster, Biophys. J. **84**, 1591 (2003).

[38] I. L. Novak, B. M. Slepchenko, and A. Mogilner, Biophys. J. **95**, 1627 (2008).

[39] H. Berg, *Random Walks in Biology* (Princeton University Press, Princeton, NJ, 1983).

[40] A. Mogilner, J. Math. Biol. **58**, 105 (2009).

[41] L. Le Goff, O. Hallatschek, E. Frey, and F. Amblard, Phys. Rev. Lett. **89**, 258101 (2002).

[42] E. Evans, Annu. Rev. Biophys. Biomol. Struct. **30**, 105 (2001).

[43] V. M. Laurent, S. Kasas, A. Yersin, T. E. Schäffer, S. Catsicas, G. Dietler, A. B. Verkhovsky, and J.-J. Meister, Biophys. J. **89**, 667 (2005).

[44] C. Brunner, A. Ehrlicher, B. Kohlstrunk, D. Knebel, J. Käs, and M. Goegler, Eur. Biophys. J. **35**, 713 (2006).

[45] T. Betz, D. Koch, D. Lim, and J. A. Käs, Biophys. J. **96**, 5130 (2009).

[46] S. S. Palecek, J. C. Loftus, M. H. Ginsberg, D. A. Lauffenburger, and A. F. Horwitz, Nature (London) **385**, 537 (1997).

[47] S. H. Parekh, O. Chaudhuri, J. A. Theriot, and D. A. Fletcher, Nat. Cell Biol. **7**, 1219 (2005).

[48] K. Keren, Z. Pincus, G. M. Allen, E. L. Barnhart, G. Marriott, A. Mogilner, and J. A. Theriot, Nature (London) **453**, 475 (2008).